Cerium(III) and Cerium(IV) Bis(η^8-pentalene) Sandwich Complexes: Synthetic, Structural, Spectroscopic, and Theoretical Studies

Gabor Balazs,[‡] F. Geoffrey N. Cloke,*[,†] Jennifer C. Green,*[,‡] Robert M. Harker,[†] Andrew Harrison,[§,⊥] Peter B. Hitchcock,[†] Christian N. Jardine,[‡] and Richard Walton[‡]

The Chemistry Department, School of Life Sciences, University of Sussex, Brighton, BN1 9QJ, U.K., Inorganic Chemistry Laboratory, University of Oxford, South Parks Road, Oxford, OX1 3QR, U.K., School of Chemistry, University of Edinburgh, Joseph Black Building, West Mains Road, Edinburgh, Scotland EH9 3JJ, and Institut Laue-Langevin, 6 Rue Jules Horowitz, BP 156−38042, Grenoble Cedex 9, France

Received March 22, 2007

The Ce(III) anionic bis(pentalene) sandwich complex K[Ce{$C_8H_4(Si^iPr_3$-1,4)$_2$}$_2$] (**1**) has been prepared by treatment of $CeCl_3$ with $K_2[C_8H_4(Si^iPr_3$-1,4)$_2]$ and crystallographically characterized as its 18-crown-6 complex. Oxidation of **1** with Ag[BPh_4] affords the neutral, formally Ce(IV) sandwich complex [Ce{$C_8H_4(Si^iPr_3$-1,4)$_2$}$_2$] (**2**), whose molecular structure has also been determined. The electronic structure of **2** has been investigated in detail by a combination of magnetic studies, K-edge XANES measurements, gas-phase photoelectron spectroscopy, and density functional calculations.

Introduction

There is currently considerable interest in cerium(IV) organometallic chemistry, specifically the controversy surrounding the optimal assignment of oxidation state of cerium in such complexes and the apparent incompatibility between a highly oxidizing, formally Ce(IV) metal center and easily oxidized, "soft" hydrocarbon ligands. Pre-eminent in this debate is the molecule cerocene ($CeCOT_2$, COT=η-C_8H_8), first characterized by Streitweiser et al., who reported photoelectron spectroscopic and computational studies consistent with a tetravalent formulation, i.e., a Ce^{4+} center sandwiched between two aromatic COT^{2-} dianions.[1] Raymond also argued strongly, primarily on structural grounds, for such an ionic formulation of COT-based complexes of the lanthanides and actinides.[2,3] Several recent structures of cerocenes and their anions with a variety of substituents are largely consistent with this view.[4−6] However, detailed computational studies by Dolg and co-workers on $CeCOT_2$ and its actinide analogue $ThCOT_2$ concluded that, while the ground state of $ThCOT_2$ is $^1A_{1g}$ with a dominant configuration to this state of $\pi(e_{2u})^4f^0d^0$, $CeCOT_2$, while also possessing a $^1A_{1g}$ ground state, does not have a dominant π-$(e_{2u})^4$ configuration.[7−9] In fact, this configuration was found to contribute only ∼20% to the ground-state wave function. The dominant contribution (∼80%) comes from the π-$(e_{2u})^3f_\delta{}^1$ configuration, in which the two unpaired electrons are antiferromagnetically coupled in two molecular orbitals, and the direct product of their spatial symmetries is A_{1g}. Thus, on this basis, $CeCOT_2$ is best described as having a single metal-localized valence 4f electron, i.e., as a Ce(III) compound containing two formally $COT^{1.5-}$ rings. Subsequent studies using synchrotron radiation-based X-ray absorption spectroscopy (XANES) also showed that the absorption K-edge of the cerium center in both $CeCOT_2$ and $[CeCOT_2]^-$ lies in the trivalent rather than the tetravalent range.[10] Amberger has very recently shown that optical spectroscopic properties of substituted cerocenes may be more consistent with a bonding model based on Ce(III) than Ce(IV).[11] Andersen has also discussed the bonding in $CeCOT_2$ in terms of a molecular Kondo effect, based on detailed magnetic susceptibility and L_{III}-edge X-ray absorption spectroscopy data.[12]

Cerium complexes derived from the pentalene dianion would offer an interesting comparison with the related cyclooctatetraene complexes discussed above, especially with regard to their electronic structure. We have developed a synthetic routes to 1,4-trialkylsilyl-substituted pentalene ligands[13] and reported the synthesis and molecular structure of [Th(η-$C_8H_4(Si^iPr_3$-1,4)$_2$], a pentalene analogue of $[ThCOT_2]$.[14] In this paper we describe the synthesis of the analogous anionic cerium(III) and neutral cerium(IV) pentalene sandwich complexes and a detailed study of the electronic structure and bonding in the latter.

* Corresponding authors. E-mail: f.g.cloke@sussex.ac.uk; jennifer.green@chem.ox.ac.uk.
† University of Sussex.
‡ University of Oxford.
§ University of Edinburgh.
⊥ Institut Laue-Langevin.

(1) Streitwieser, A.; Kinsley, S. A.; Rigsbee, J. T.; Fragala, I. L.; Ciliberto, E.; Rösch, N. *J. Am. Chem. Soc.* **1985**, *107*, 7786.
(2) Hodgson, K. O.; Raymond, K. N. *Inorg. Chem.* **1972**, *11*, 3030.
(3) Raymond, K. N.; Eigenbrot, C. W., Jr. *Acc. Chem. Res.* **1980**, *13*, 276.
(4) Boussie, T. R.; Eisenberg, D. C.; Rigsbee, J.; Streitwieser, A.; Zalkin, A. *Organometallics* **1991**, *10*, 1922.
(5) Kilimann, U.; Herbst-Immer, R.; Stalke, D.; Edelmann, F. T. *Angew. Chem., Int. Ed. Engl.* **1994**, *33*, 1618.
(6) Reissmann, U.; Lameyer, L.; Stalke, D.; Poremba, P.; Edelmann, F. T. *Chem. Commun.* **1999**, 1865.
(7) Dolg, M.; Fulde, P.; Kuchle, W.; Neumann, C. S.; Stoll, H. *J. Chem. Phys.* **1991**, *94*, 3011.
(8) Dolg, M.; Fulde, P.; Stoll, H.; Preuss, H.; Chang, A.; Pitzer, R. M. *J. Chem. Phys.* **1995**, *195*, 71.
(9) Liu, W. J.; Dolg, M.; Fulde, P. *J. Chem. Phys.* **1997**, *107*, 3584.
(10) Edelstein, N. M.; Allen, P. G.; Bucher, J. J.; Shuh, D. K.; Sofield, C. D.; Kaltsoyannis, N.; Maunder, G. H.; Russo, M. R.; Sella, A. *J. Am. Chem. Soc.* **1996**, *118*, 13115.
(11) Amberger, H. D.; Reddmann, H.; Edelmann, F. T. *J. Organomet. Chem.* **2005**, *690*, 2238.
(12) Booth, C. H.; Walter, M. D.; Daniel, M.; Lukens, W. W.; Andersen, R. A. *Phys. Rev. Lett.* **2005**, *95*, 267202.
(13) Cloke, F. G. N.; Kuchta, M. C.; Harker, R. M.; Hitchcock, P. B.; Parry, J. S. *Organometallics* **2000**, *19*, 5795.
(14) Cloke, F. G. N.; Hitchcock, P. B. *J. Am. Chem. Soc.* **1997**, *119*, 7899.

10.1021/om7002738 CCC: $37.00
Publication on Web 05/23/2007

Experimental Section

General Methods. Unless otherwise stated, all experimental procedures were carried out using standard high-vacuum and Schlenk techniques, under an atmosphere of dry argon (manipulation of **1** requires Ar of 99.999+% purity) or under dinitrogen in an MBraun or a Miller-Howe glovebox. Glassware was flame dried under vacuum prior to use, and Celite filter aid was predried in an oven at 200 °C. *n*-Pentane and diethyl ether were distilled from sodium/potassium alloy, tetrahydrofuran and toluene were distilled from potassium metal, and pyridine was distilled from CaH_2 under dinitrogen prior to use; toluene-d_8 was dried over molten potassium, then vacuum transferred to, and stored in, an ampule under dinitrogen prior to use. NMR spectra were recorded at 295 K on a Bruker DPX 300 MHz spectrometer, with chemical shifts (δ) reported in ppm, relative to the chemical shifts of the internal deuterated solvent (^1H and ^{13}C) set relative to external TMS. Coupling constants are quoted in Hz. Electron impact mass spectra were recorded on a VG Autospec mass spectrometer. Magnetic measurements on **1** and **2** were carried out on a Quantum Design SQUID magnetometer in O-ring-sealed KelF capsules at fields of 0.1 and 1 T over the temperature range 5−340 K.

Elemental analyses were carried out by Mikroanalytisches Labor Pascher, Remagen, Germany, and the University of North London Elemental Analysis Service, London, UK.

Anhydrous $CeCl_3$ was prepared from $CeCl_3 \cdot 6H_2O$ using trimethylsilyl chloride according to the method of Boudjouk.[15] $AgBPh_4$ was prepared by precipitation from aqueous solutions of silver nitrate and sodium tetraphenylborate, followed by drying under vacuum. 18-Crown-6 was purified by precipitation from acetonitrile, drying under vacuum, and recrystallization from heptane. $K_2[C_8H_4(Si^iPr_3\text{-}1,4)_2]$[13] and $[Ce(\eta\text{-}C_8H_5(SiMe_3\text{-}1,3,5)_3)_2]$ ($Ce(COT'''')_2$)[3] were prepared as described elsewhere.

XANES Experiments. XANES data were measured at the cerium K-edge (~40.443 keV) on Station 9.2 of the Daresbury SRS. The synchrotron operates with an average stored energy of 2 GeV and a typical electron current of 200 mA. The incident X-ray energy on the sample was selected using a double-crystal Si(220) monochromator, and the second crystal of the monochromator was detuned to 90% of the maximum intensity to reduce contributions from higher order harmonics of the selected wavelength. Data were collected in transmission mode from the cerium-containing materials, with incident and transmitted X-ray intensities measured using ionization chambers filled with appropriate quantities of noble gas. The beam was defined as a 12 mm horizontal slit. Data were measured from a CeB_6 standard simultaneously with each sample to provide a calibration; this was placed between the transmitted ionization chamber and third ionization chamber. Solutions of $Ce(COT'''')_2$ (0.3 M in toluene), **1** (0.06 M in THF), and **2** (0.03 M in toluene) were contained in sealed NMR tubes, and solid samples of CeO_2 and CeB_6 were pressed into self-supporting discs with ~50% by mass polyethylene powder. The Ce K-edge region was scanned from 40.25 to 40.65 keV, and four scans from each sample and from CeO_2 were taken. Although the intrinsic resolution of experiment, which broadens the features of the XANES region, is on the order of 10 eV, the precision of the edge energy positions can be determined with much greater accuracy, as previously pointed out.[10] The data were normalized and summed using the program EXCALIB, and analysis was performed using the program EXBACK.[16] The edge position was defined as the point of inflection of the near edge region and determined by measuring the position of the maximum of the first derivative of X-ray absorption data.

DFT Computational Studies. Density functional calculations were carried out using the Gaussian 03 package[17] with the hybrid B3LYP[18,19] functional using the 6-31++G* basis sets[20−26] for C and H and the Dunning/Huzinaga[27] type basis set with the Stuttgart/Dresden pseudorelativistic core potential for Ce.[28] For fragment calculations the Amsterdam Density Functional program suite ADF 2005.01 was used.[29,30] Scalar relativistic corrections were included via the ZORA method.[31−35] The generalized gradient approximation was employed, using the local density approximation of Vosko, Wilk, and Nusair[36,37] together with the nonlocal exchange correction by Becke[38,39] and nonlocal correlation corrections by Perdew.[40] TZP basis sets were used with triple-accuracy sets of Slater-type orbitals and two polarization functions added to the main group atoms. A post-SCF gradient correction was applied.

The geometries of $[Ce(C_8H_6)_2]$ were optimized in the D_2, D_{2d}, and D_{2h} point groups. The optimized geometry within the restraints of the D_2 point group has D_{2d} symmetry. Vertical ionization energies were estimated, using the optimized structure, from the difference between the total energy for the molecule and that for the molecular ion in the appropriate state. For the geometry optimizations in Gaussian 6-31++G* basis sets for C and H and SDD for Ce together with the pseudorelativistic core potential of first 28 electrons of Ce were used.

(15) So, J.-H.; Boudjouk, P. *Inorg. Chem.* **1990**, *29*, 1592.
(16) Binsted, N.; Campbell, J. W.; Gurman, S. J.; Stephensen, P. C. *EXBACK*, Daresbury, 1999.
(17) Frisch, M. J.; Trucks, G. W.; Schlegel, H. B.; Scuseria, G. E.; Robb, M. A.; Cheeseman, J. R.; Montgomery, J. A.; Vreven, T.; Kudin, K. N.; Burant, J. C.; Millam, J. M.; Iyengar, S. S.; Tomasi, J.; Barone, V.; Mennucci, B.; Cossi, M.; Scalmani, G.; Rega, N.; Petersson, G. A.; Nakatsuji, H.; Hada, M.; Ehara, M.; Toyota, K.; Fukuda, R.; Hasegawa, J.; Ishida, M.; Nakajima, T.; Honda, Y.; Kitao, O.; Nakai, H.; Klene, M.; Li, X.; Knox, J. E.; Hratchian, H. P.; Cross, J. B.; Bakken, V.; Adamo, C.; Jaramillo, J.; Gomperts, R.; Stratmann, R. E.; Yazyev, O.; Austin, A. J.; Cammi, R.; Pomelli, C.; Ochterski, J. W.; Ayala, P. Y.; Morokuma, K.; Voth, G. A.; Salvador, P.; Dannenberg, J. J.; Zakrzewski, V. G.; Dapprich, S.; Daniels, A. D.; Strain, M. C.; Farkas, O.; Malick, D. K.; Rabuck, A. D.; Raghavachari, K.; Foresman, J. B.; Ortiz, J. V.; Cui, Q.; Baboul, A. G.; Clifford, S.; Cioslowski, J.; Stefanov, B. B.; Liu, G.; Liashenko, A.; Piskorz, P.; Komaromi, I.; Martin, R. L.; Fox, D. J.; Keith, T.; Al-Laham, M. A.; Peng, C. Y.; Nanayakkara, A.; Challacombe, M.; Gill, P. M. W.; Johnson, B.; Chen, W.; Wong, M. W.; Gonzalez, C.; Pople, J. A. *Gaussian 03, Revision C.02*; Gaussian, Inc.: Wallingford, CT, 2004.
(18) Lee, C.; Yang, W.; Parr, R. G. *Phys. Rev. B* **1988**, *37* (2), 785.
(19) Miehlich, B.; Savin, A.; Stoll, H.; Preuss, H. *Chem. Phys. Lett.* **1989**, *157*, 200.
(20) Ditchfield, R.; Hehre, W. J.; Pople, J. A. *J. Chem. Phys.* **1971**, *54* (2), 724.
(21) Francl, M. M.; Pietro, W. J.; Hehre, W. J.; Binkley, J. S.; Gordon, M. S.; DeFrees, D. J.; Pople, J. A. *J. Chem. Phys.* **1982**, *77* (7), 3654.
(22) Hariharan, P. C.; Pople, J. A. *Theor. Chim. Acta* **1973**, *28* (3), 213.
(23) Hariharan, P. C.; Pople, J. A. *Mol. Phys.* **1974**, *27*, 209.
(24) Hehre, W. J.; Ditchfield, R.; Pople, J. A. *J. Chem. Phys.* **1972**, *56* (5), 2257.
(25) Rassolov, V. A.; Pople, J. A.; Ratner, M. A.; Windus, T. L. *J. Chem. Phys.* **1998**, *109* (4), 1223.
(26) Rassolov, V. A.; Ratner, M. A.; Pople, J. A.; Redfern, P. C.; Curtiss, L. A. *J. Comput. Chem.* **2001**, *22* (9), 976.
(27) Dunning, T. H.; Hay, P. J. In *Modern Theoretical Chemistry*; Plenum: New York, 1976; Vol. 3, pp 1−28.
(28) Cao, X.; Dolg, M. *THEOCHEM* **2002**, *581*, 139.
(29) Te Velde, G.; Bickelhaupt, F. M.; Baerends, E. J.; Fonseca Guerra, C.; Van Gisbergen, S. J. A.; Snijders, J. G.; Ziegler, T. *J. Comput. Chem.* **2001**, *22*, 931.
(30) Fonseca Guerra, C.; Snijder, J. G.; Te Velde, G.; Baerends, E. J. *Theor. Chem. Acc.* **1998**, *99*, 391.
(31) van Lenthe, E.; Baerends, E. J.; Snijders, J. G. *J. Chem. Phys.* **1993**, *99*, 4597.
(32) van Lenthe, E.; Baerends, E. J.; Snijders, J. G. *J. Chem. Phys.* **1994**, *101*, 9783.
(33) van Lenthe, E.; Baerends, E. J.; Snijders, J. G. *J. Chem. Phys.* **1996**, *105*, 6505.
(34) van Lenthe, E.; Ehlers, A.; Baerends, E. J. *J. Chem. Phys.* **1999**, *110*, 8943.
(35) van Lenthe, E.; van Leeuwen, R.; Baerends, E. J.; Snijders, J. G. *Int. J. Quantum. Chem.* **1996**, *57*, 281.
(36) Vosko, S. H.; Wilk, L.; Nusair, M. *Can. J. Phys.* **1980**, *58*, 1200.
(37) Vosko, S. H.; Wilk, L.; Nusair, M. *Can. J. Phys.* **1980**, *58*, 1200.
(38) Becke, A. D. *Phys. Rev. A* **1988**, *38*, 3098.
(39) Becke, A. D. *J. Chem. Phys.* **1988**, *88*, 1053.
(40) Perdew, J. P. *Phys. Rev. B* **1986**, *33*, 8800.

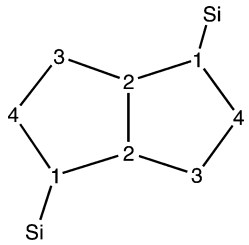

Figure 1. Ring-numbering scheme for NMR assignments.

Photoelectron Spectroscopy. Photoelectron spectra were measured using a PES laboratories 0078 spectrometer interfaced with an Atari microprocessor. Spectra were calibrated with He, Xe, and N_2. In order to obtain a suitable vapor pressure, the sample was held at a temperature of 236 °C.

Preparation of [Ce{$C_8H_4(Si^iPr_3$-1,4)$_2$}$_2$]$^-$[K(18-crown-6)]$^+$, 1. THF (50 cm^3) was added to a stirred mixture of solid $CeCl_3$ (0.26 g, 1.05 mmol) and $K_2[C_8H_4(Si^iPr_3\text{-}1,4)_2]$ (1.03 g, 2.08 mmol). The gold-colored mixture was stirred at room temperature for 18 h to give a darker brown mixture. The reaction mixture was filtered through Celite on a frit and washed through with a further 20 mL of THF. Initial contact of the reaction mixture with the frit caused the first few drops of solution to turn an intense blue color (due to trace oxidation to **2**); however the remainder of the mixture filtered to a clear golden-brown solution. Solvent was removed in a vacuum to give a greenish-brown solid, which was washed on a frit until pentane washings, which were initially blue, became colorless. The crude $K[Ce\{C_8H_4(Si^iPr_3\text{-}1,4)_2\}_2]$ was again dried in a vacuum to give a sand-colored powder, yield 0.71 g (68%). Toluene (7 mL) was added to a mixture of crude $K[Ce\{C_8H_4(Si^iPr_3\text{-}1,4)_2\}_2]$ (0.189 g, 0.19 mmol) and 18-crown-6 (0.050 g, 0.19 mmol) in an ampule. Agitation of the mixture resulted in a yellow solution containing a brown oil that crystallized after storing at 4 °C for several weeks. The solution was decanted from the crystals, and the product was washed with pentane, dried in a vacuum, and recrystallized from hot toluene to afford pure **1**. Anal. Calcd for $[C_{64}H_{116}CeKO_6Si_4]$: C, 60.38; H, 9.18. Found: C, 59.95; H, 9.03.

Crystals suitable for single-crystal X-ray diffraction were obtained by vapor diffusion of pentane into a saturated solution of **1** in pyridine.

Preparation of [Ce{$C_8H_4(Si^iPr_3$-1,4)$_2$}$_2$] 2. A prereacted mixture of $CeCl_3$ (0.25 g, 1.0 mmol) and $K_2[C_8H_4(Si^iPr_3\text{-}1,4)_2]$ (0.98 g, 2.0 mmol) in THF (50 cm^3) was added to a slurry of $AgBPh_4$ (0.43 g, 1.0 mmol) in THF (20 cm^3), which resulted in an immediate color change from red to deep blue. After stirring for 24 h the solvent was removed in a vacuum and the product extracted with pentane. Filtration of the dark blue solution, concentration, and cooling to −45 °C for 3 days resulted in very dark blue crystals of **2**, which were washed in cold pentane and dried in a vacuum. Yield: 0.81 g (80%). Anal. Calcd for $[C_{52}H_{92}CeSi_4]$: C, 64.40; H, 9.56. Found: C, 64.38; H, 9.86. MS (EI, 70 eV): *m*/*e* 968 (M^+, 20%). ^{1}H NMR (300 MHz, C_7D_8, 295 K, assignments in Figure 1): δ 7.21 (1.9H, d, J = 3.0 Hz, A4), 5.92 (1.6H, d, J = 3.0 Hz, B4), 3.04 (1.5H, d, J = 3.0 Hz, B3), 1.43 (11.3H, overlapping septets, A+B SiC*H*{CH_3}$_2$), 1.23 (66.6H, overlapping doublets, A+B SiCH{C*H*$_3$}$_2$), 0.24 (2.0H, d, J = 3.0 Hz, A3). ^{13}C{^{1}H} NMR (75.5 MHz, C_7D_8, 295 K, assignments in Figure 1): δ 169.11 (A1), 155.26 (A3), 152.46 (B2), 145.71 (B1), 136.68 (B3), 135.62 (A2), 123.23 (B4), 107.05 (A4), 20.06 (^{i}PrCH$_3$), 19.74 (^{i}PrCH$_3$), 19.63 (^{i}PrCH$_3$), 19.35 (^{i}PrCH$_3$), 17.59 (^{i}PrCH), 15.49 (^{i}PrCH).

X-ray Data Collection, Structure Solution, and Refinement. Data collection was performed at 173(2) K on an Enraf-Nonius Kappa CCD diffractometer, with graphite-monochromated Mo Kα radiation (λ = 0.71073 Å). The molecular structure was solved by direct methods and refined on F^2 by full-matrix least-squares techniques.

Results and Discussion

Synthetic Studies. The reaction of $CeCl_3$ with 2 equiv of $K_2[C_8H_4(Si^iPr_3\text{-}1,4)_2]$ in THF afforded tan-colored $K[Ce\{C_8H_4(Si^iPr_3\text{-}1,4)_2\}_2]$ in ca. 70% yield after workup. $K[Ce\{C_8H_4(Si^iPr_3\text{-}1,4)_2\}_2]$ is exceptionally sensitive to aerial oxidation, even minute traces of air resulting in the formation of a blue color attributed to **2** (*vide infra*). Treatment of crude $K[Ce\{C_8H_4(Si^iPr_3\text{-}1,4)_2\}_2]$ with 18-crown-6 in toluene yielded analytically pure, crystalline $[Ce\{C_8H_4(Si^iPr_3\text{-}1,4)_2\}_2]$-[K(18-crown-6)] (**1**) after recrystallization from hot toluene (see Scheme 1).

Oxidation of *in situ*-generated $K[Ce\{C_8H_4(Si^iPr_3\text{-}1,4)_2\}_2]$ with 1 equiv of $Ag[BPh_4]$ in THF resulted in formation of an intense blue solution, from which blue-black crystals of the Ce(IV) complex $[Ce\{C_8H_4(Si^iPr_3\text{-}1,4)_2\}_2]$ (**2**) could be isolated (see Scheme 1) after recrystallization from pentane; **2** may also be purified by sublimation at 250 °C/10^{-5} mbar. The UV spectrum of **2** in pentane solution displays a strong band ($\epsilon = 5 \times 10^3$ M^{-1} cm^{-1}) at 590 nm, assignable to a LMCT transition.

2 exhibits ^{1}H and ^{13}C NMR solution spectra with sharp bands as expected for a diamagnetic complex; HOESY experiments allowed assignment of the ring protons and carbons for the mixture of isomers, but could not distinguish between the isomers. The ring-numbering scheme for chemical shift assignments is shown in Figure 1 (the top and bottom rings in isomer A and in isomer B are related by symmetry in solution).

The chemical shifts of the "wingtip" protons A4 and B4 (for the two isomers A and B) are in a region of the spectrum similar to those of $[Th(\eta\text{-}C_8H_4(Si^iPr_3\text{-}1,4)_2]$[14] and are essentially temperature invariant. However, interestingly, the other ring protons A3 and B3 occur at significantly higher field than those in the thorium analogue, and their chemical shifts move to higher field with increasing temperature (by ca. 0.5 ppm over the temperature range 185−385 K). The respective ^{13}C resonances do not change. Variable-temperature (185−385 K) ^{13}C NMR studies revealed no significant changes in J_{CH} values indicative of any low-temperature agostic interactions. We deduce that there is a significant paramagnetic contribution to the shielding arising from the Ce center. This deduction is supported by the temperature-independent paramagnetic (TIP) contribution to the susceptibility and the small HOMO−LUMO gap (*vide infra*). Such shielding, analogous to that of transition metal hydrides, is known to be potentially highly directional.[41] The small

Scheme 1

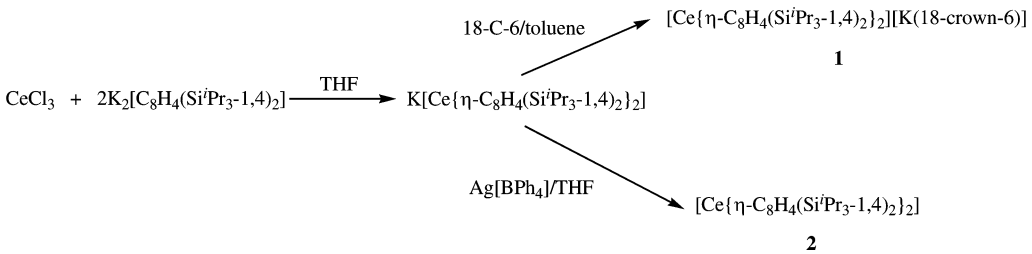

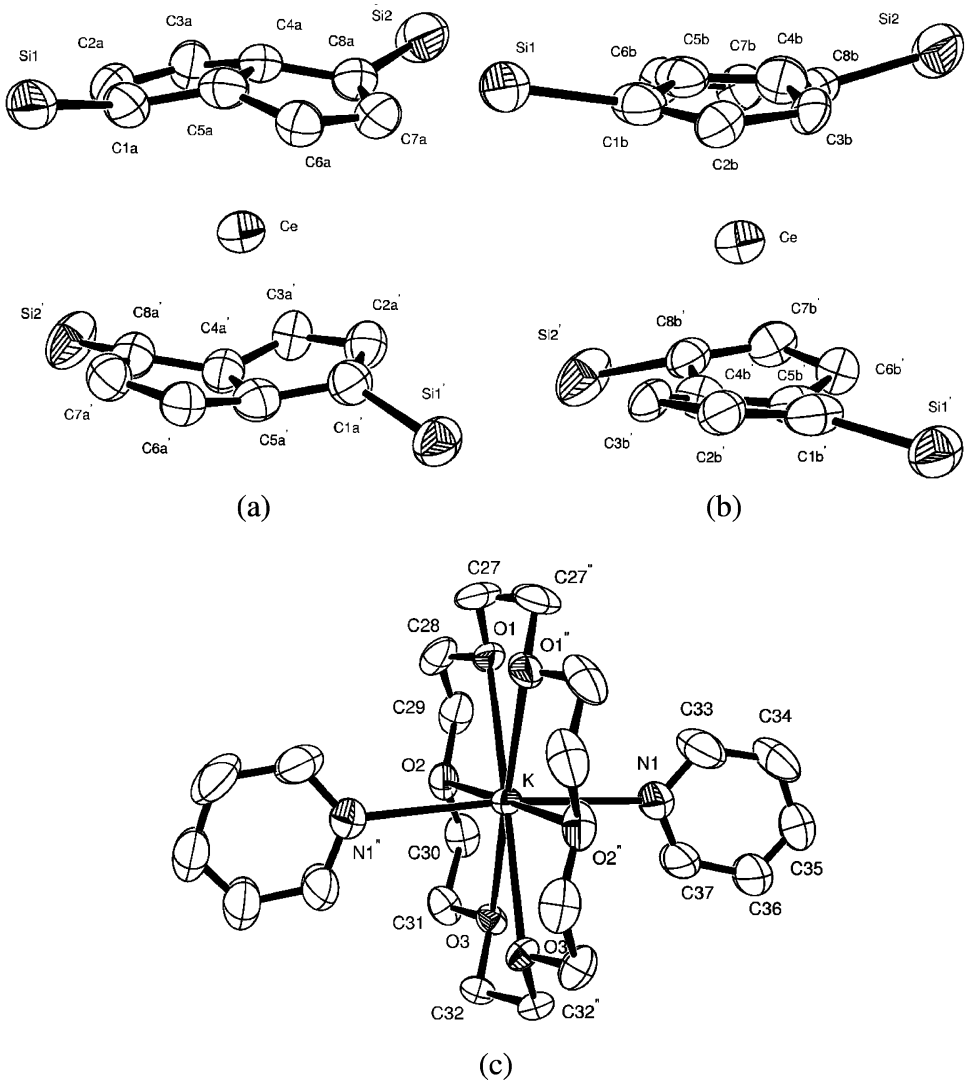

Figure 2. Molecular structure of **1**·(pyridine)$_2$ (thermal ellipsoids at 20%). The isopropyl groups have been omitted for clarity.

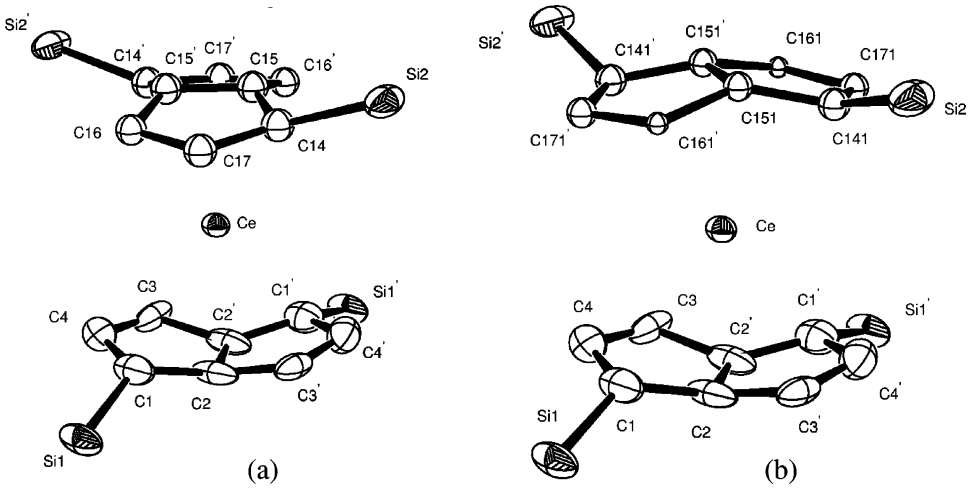

Figure 3. Molecular structure of **2** (thermal ellipsoids at 20%). The isopropyl groups have been omitted for clarity.

temperature variations are likely to be due to thermal motion between conformers (see Structural Studies).

Structural Studies. Crystals of **1** suitable for X-ray diffraction were obtained by vapor diffusion of pentane into a saturated solution of **1** in pyridine, and those of **2** were grown by slow cooling of a saturated solution of **2** in pentane; the structures are shown in Figures 2 and 3, respectively, with selected bond distances and angles in Table 2.

The structure of **1** shows a (disorded, *vide infra*) bis(η^8-pentalene)cerium anion with a remote K(18-crown-6)(pyridine)$_2$ cation (Figure 2c). In the latter, the potassium atom lies in the

(41) Buckingham, A. D.; Stephens, P. J. *J. Chem. Soc.* **1964**, *2747*, 4583.

Table 1. X-ray Data Collection Parameters for 1 and 2

	1·(pyridine)$_2$	**2**·(pentane)
formula	$C_{74}H_{126}CeKN_2O_6Si_4$	$C_{52}H_{92}CeSi_4$
fw	1431.35	1041.88
space group	$I4_1/acd$ (No. 142)	$C2/c$ (No. 15)
a, Å	24.6965(2)	21.308(4)
b, Å	24.6965(2)	13.376(5)
c, Å	53.5110(5)	21.109(5)
α, deg	90	90
β, deg	90	95.93(2)
γ, deg	90	90
V, Å^3	32637.3(5)	5984(3)
Z	16	4
ρ_{calc}, g/cm^3	1.16	1.16
T, K	173	173
μ(Mo Kα), mm^{-1}	0.71	0.87
θ range for data collection, deg	4.28−25.01	2.09−22.99
total no. of data	110 448	4269
no. of unique data	7140	4150
no. of reflns with $I > 2\sigma(I)$	5432	3831
no. of data/restraints/params	7140/28/472	4150/6/279
R1 [$I > 2\sigma(I)$]	0.050	0.037
wR2 [$I > 2\sigma(I)$]	0.122	0.096
max., min. peaks, e/Å^3	0.67, −0.41	1.21, −1.05

center of the crown ether ligand with K−O distances (2.787(5)−2.811(4) Å) in the expected region. Axial pyridine molecules complete the coordination sphere of the potassium with the K−N distances at 2.868(6) Å and a N−K−N angle of 174.3(3)°.

The 1,4-bis(silylated) pentalene dianion has C_2-symmetry and is facially enantiotopic; thus a sandwich compound incorporating two such ligands would be expected to exist, in principle, in four diastereomeric forms (meso and racemic isomers of the staggered and of the eclipsed sandwich structures). However, two possible diastereoisomers (the chiral form of the staggered isomer and the meso form of the eclipsed isomer) are expected to be precluded on steric grounds, due to unfavorable interactions between the silyl ring substituents. This has been previously observed in the structure of [Th(η-C_8H_4(Si^{i}Pr$_3$-1,4)$_2$], which exists as distinct, noninterconvertible staggered (meso form) and semieclipsed (chiral form) isomers.[14] These isomers coexist in a single crystal of [Th(η-C_8H_4(Si^{i}Pr$_3$-1,4)$_2$], manifest in a disorder of the pentalene framework, an effect ascribed to domination of the crystal-packing forces by the bulky triisopropylsilyl groups, whose disposition is virtually identical in both isomers. The disorder was modeled by a 52%:48% occupancy of the two pentalene ring orientations, i.e., staggered (meso form) and semieclipsed (chiral form) isomers. Since the bis(η^8-pentalene)cerium sandwich structures in both **1** and **2** exhibit the same disorder and resultant gross features as [Th(η-C_8H_4(Si^{i}Pr$_3$-1,4)$_2$], they will now be discussed together.

In **1** the twist angles (as defined by the angles between the two bridgehead C−C vectors) of the two pentalene rings are 44° for the semistaggered isomer (66% occupancy, Figure 2a) and 10° for the virtually eclipsed isomer (34% occupancy, Figure 2b). Corresponding values for **2** are 85° for the virtually staggered isomer (72% occupancy, Figure 3a) and 33° for the semieclipsed isomer (28% occupancy, Figure 3b), twist angles

Table 2. Bond Distances and Angles in 1 and 2

1·(pyridine)$_2$		**2**		**1**·(pyridine)$_2$		**2**	
Distances (Å) within Rings				Angles (deg) within Rings			
C(1A)−C(2A)	1.423(10)	C(1)−C(2)	1.409(7)	C(2A)−C(1A)−C(5A)	104.3(6)	C(2)−C(1)−C(4)	102.2(4)
C(1A)−C(5A)	1.448(8)	C(1)−C(4)	1.444(7)	C(3A)−C(2A)−C(1A)	112.7(10)	C(2)′−C(2)−C(1)	114.1(6)
C(2A)−C(3A)	1.417(11)	C(2)−C(2)′	1.396(9)	C(2A)−C(3A)−C(4A)	105.4(12)	C(2)′−C(2)−C(3)′	104.1(5)
C(3A)−C(4A)	1.460(17)	C(2)−C(3)′	1.473(7)	C(5A)−C(4A)−C(8A)	111.5(7)	C(1)−C(2)−C(3)′	135.1(4)
C(4A)−C(5A)	1.429(10)	C(3)−C(4)	1.366(7)	C(5A)−C(4A)−C(3A)	107.5(8)	C(4)−C(3)−C(2)′	107.3(4)
C(4A)−C(8A)	1.452(9)	C(3)−C(2)′	1.473(7)	C(8A)−C(4A)−C(3A)	135.0(10)	C(4)−C(3)−Ce	82.5(3)
C(5A)−C(6A)	1.422(14)	C(5)−C(6)	1.496(8)	C(6A)−C(5A)−C(4A)	106.5(7)	C(3)−C(4)−C(1)	112.3(4)
C(6A)−C(7A)	1.410(11)	C(5)−C(7)	1.519(8)	C(6A)−C(5A)−C(1A)	137.3(8)	C(17)−C(14)−C(15)	104.4(5)
C(7A)−C(8A)	1.434(9)	C(8)−C(9)	1.509(9)	C(4A)−C(5A)−C(1A)	110.1(7)	C(16)′−C(15)−C(15)′	108.1(6)
C(1B)−C(2B)	1.415(14)	C(8)−C(10)	1.534(8)	C(7A)−C(6A)−C(5A)	107.2(10)	C(16)′−C(15)−C(14)	135.9(5)
C(1B)−C(5B)	1.446(12)	C(11)−C(12)	1.520(8)	C(6A)−C(7A)−C(8A)	112.7(8)	C(15)′−C(15)−C(14)	109.3(6)
C(2B)−C(3B)	1.439(15)	C(11)−C(13)	1.526(7)	C(7A)−C(8A)−C(4A)	102.1(6)	C(17)−C(16)−C(15)′	105.8(5)
C(3B)−C(4B)	1.46(2)	C(18)−C(19)	1.528(7)	C(2B)−C(1B)−C(5B)	104.3(10)	C(14)−C(17)−C(16)	112.2(5)
C(4B)−C(5B)	1.435(14)	C(18)−C(20)	1.530(7)	C(1B)−C(2B)−C(3B)	112.9(13)	C(171)−C(141)−C(151)	104.6(9)
C(4B)−C(8B)	1.446(14)	C(21)−C(22)	1.516(9)	C(2B)−C(3B)−C(4B)	104.9(16)	C(141)−C(151)−C(151)′	110.9(13)
C(5B)−C(6B)	1.41(2)	C(21)−C(23)	1.525(9)	C(5B)−C(4B)−C(8B)	110.7(11)	C(141)−C(151)−C(161)′	136.2(12)
C(6B)−C(7B)	1.420(16)	C(24)−C(26)	1.520(7)	C(5B)−C(4B)−C(3B)	107.5(12)	C(151)′−C(151)−C(161)′	105.9(12)
C(7B)−C(8B)	1.423(14)	C(24)−C(25)	1.522(7)	C(8B)−C(4B)−C(3B)	136.2(14)	C(171)−C(161)−C(151)′	105.3(10)
		C(14)−C(17)	1.418(7)	C(6B)−C(5B)−C(4B)	106.6(11)	C(141)−C(171)−C(161)	113.1(8)
		C(14)−C(15)	1.442(7)	C(6B)−C(5B)−C(1B)	138.2(14)		
		C(15)−C(16)′	1.425(8)	C(4B)−C(5B)−C(1B)	110.4(11)		
		C(15)−C(15)′	1.435(11)	C(5B)−C(6B)−C(7B)	107.7(15)		
		C(16)−C(17)	1.420(8)	C(6B)−C(7B)−C(8B)	111.4(12)		
		C(16)−C(15)′	1.425(8)	C(7B)−C(8B)−C(4B)	103.6(10)		
		C(141)−C(171)	1.415(12)	Ce−Ring Distances (Å)			
		C(141)−C(151)	1.425(14)	Ce−C(1A)	2.844(7)	Ce−C(2)	2.495(4)
		C(151)−C(151)′	1.46(2)	Ce−C(2A)	2.960(7)	Ce−C(15)	2.496(6)
		C(151)−C(161)′	1.464(17)	Ce−C(3A)	2.824(19)	Ce−C(151)	2.518(13)
		C(161)−C(171)	1.433(14)	Ce−C(4A)	2.592(11)	Ce−C(3)	2.730(4)
		C(161)−C(151)′	1.464(17)	Ce−C(5A)	2.586(6)	Ce−C(16)	2.735(5)
				Ce−C(6A)	2.836(15)	Ce−C(161)	2.760(11)
				Ce−C(7A)	2.991(7)	Ce−C(1)	2.783(4)
				Ce−C(8A)	2.895(6)	Ce−C(14)	2.784(5)
				Ce−C(1B)	2.887(12)	Ce−C(141)	2.796(13)
				Ce−C(2B)	2.921(11)	Ce−C(17)	2.886(5)
				Ce−C(3B)	2.70(3)	Ce−C(4)	2.889(4)
				Ce−C(4B)	2.47(2)	Ce−C(171)	2.925(8)
				Ce−C(5B)	2.566(12)		
				Ce−C(6B)	2.88(3)		
				Ce−C(7B)	2.956(12)		
				Ce−C(8B)	2.754(11)		
				Fold Angles (deg)			
				22 (a), 21 (b)		23	
				Twist Angles (deg)			
				44 (a), 10 (b)		85 (a), 33 (b)	

comparable to those found in [Th(η-C_8H_4(Si^{i}Pr$_3$-1,4)$_2$] (83° and 38°, respectively).

Pentalene ring carbon−carbon bond lengths (1.410(11)−1.460(17) Å) in **1** and **2** fall within the range observed in [Th{C_8H_4(Si^{i}Pr$_3$-1,4)$_2$}$_2$] (1.36(2) to 1.49(2) Å),[14] with carbon−carbon bridgehead distances (1.429(10)−1.435(14) Å for the two isomers of **1**; 1.3969(9)−1.46(2) Å for the two isomers of **2**) also comparable, within esds, to that of 1.39(2) Å in [Th{C_8H_4(Si^{i}Pr$_3$-1,4)$_2$}$_2$].[14] Cerium−carbon bond distances in **1** and **2** range from 2.47(2) Å at the bridgehead to 2.991(7) Å at the wingtips of the pentalene ligand, almost identical, within esds, to the corresponding distances in [Th{C_8H_4(Si^{i}Pr$_3$-1,4)$_2$}$_2$] (2.543(10) and 2.908(11) Å, respectively).[14] Remaining Ce−C distances in **1** and **2** lie in the range 2.70(3)−2.895(6) Å, and these compare well with those in [Th{C_8H_4(Si^{i}Pr$_3$-1,4)$_2$}$_2$] (2.748(10)−2.797(11) Å) and with those found in organosilyl-substituted cyclopentadienyl cerium(III) compounds, such as [Ce(η-C_5H_3{$SiMe_3$}$_2$-1,3)$_3$] (average Ce−C distance 2.83 Å).[42]

An important metrical parameter with respect to η^8-bound pentalene ligands is the fold angle of the pentalene framework about the bridgehead C−C bond, which can be inversely correlated with the size of the bound metal center.[43] The fold angles of 22° and 21° in the two isomers of **1** are slightly less than that observed in [Th{C_8H_4(Si^{i}Pr$_3$-1,4)$_2$}$_2$] (24°).[14] However, the temptation to attribute this to the relative sizes of Ce^{3+} (1.07 Å) versus Th^{4+} (0.99 Å) should be tempered with the fact that the pentalene ligands in both isomers of **2** are folded by 23° (Ce^{4+} radius 0.94 Å). Statistical uncertainties in the fold angles make such comparisons difficult with central metals of similar size, but the fold angles in **1** and **2** are clearly smaller than that in [Ta(C_8H_4{$SiMe_3$-1,4}$_2$)Cl_3] (33°, Ta^{5+} radius 0.64 Å).

Magnetic Studies. The solid-state magnetic susceptibility of **1** was determined over the temperature range 5−340 K, at a field of 0.1T. **1** displays Curie behavior over the range 6−150 K with $\mu_{eff} = 2.19\ \mu_B$ at 300 K, a value approaching that for a free f^1 ion (2.54 μ_B) and comparable with that found in [Ce(η-^{t}BuC_5H_4)$_3$] (2.28 μ_B at 300 K).[42]

The magnetic susceptibility of **2** and the diamagnetic thorium analogue was also determined at fields of 0.1 and 1.0 T over the temperature range 5−340 K. Changing the field over this range had no significant influence on the susceptibility over this range, and Figure 4a displays the molar values of susceptibility in a field of 1 T over the range for both materials. The response of the Th compound suggests an unexpected paramagnetic component that most likely arises from the sample holder. The same figure also displays the response of the sample holder scaled in the same manner as the sample **2** (i.e., the susceptibility was multiplied by the factor (molecular weight/sample mass) for sample **2**). Compound **2** has a higher susceptibility than the Th analogue. The contribution of the Ce in **2** to the susceptibility was therefore calculated by subtracting the response of the Th compound, and then the difference in the scaled response of the sample holder, according to the mass of the sample holder used. Figure 4b shows the resultant susceptibility after correction. This led to a residual paramagnetic component that could be fitted to a Curie−Weiss expression with negligible Weiss constant and a Curie constant of 0.003-(3) emu mol^{-1} (Ce). It is likely that the paramagnetic tail that is evident in Figure 3b is due to an error in correction for the sample holder or, alternatively, a trace paramagnetic impurity,[12] in which case the Ce component shows TIP with a molar susceptibility of $(4.5 \pm 0.3) \times 10^{-4}$ emu mol^{-1}, significantly larger than that estimated for cerocene ($(1.4 \pm 0.2) \times 10^{-4}$ emu mol^{-1}).[12] This may be accounted for by the smaller HOMO−LUMO gap in the pentalene complex.

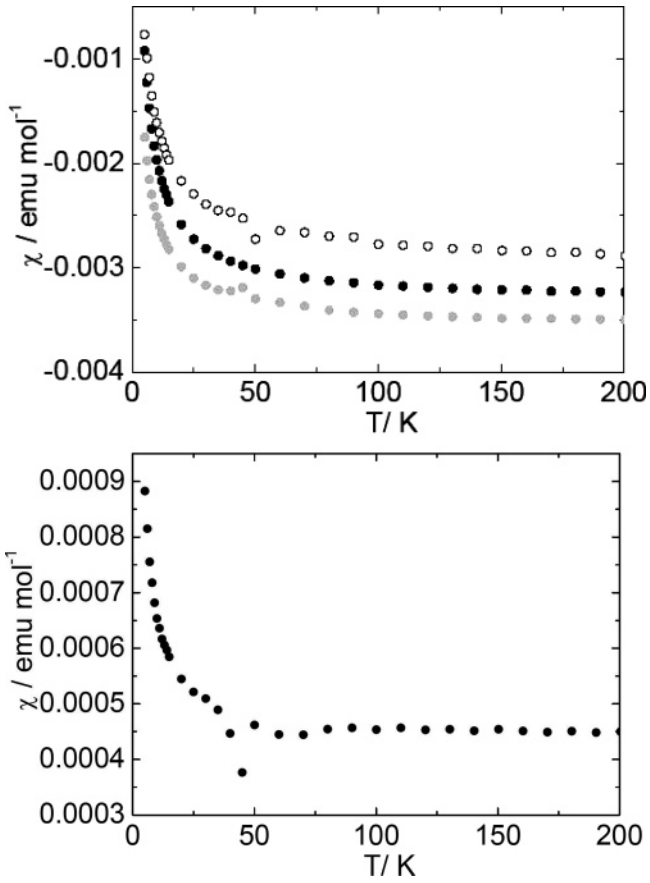

Figure 4. (a) Detail of the magnetic susceptibility of compound **2** (black circles), the thorium analogue (gray circles), and the sample holder (open circles), over the temperature range 5−200 K. The susceptibility of the sample holder has been scaled up by the same factor used to convert the measured to the molar susceptibility for **2**. (b) Residual molar susceptibility of **2** after correction for the diamagnetism of the sample and the sample holder.

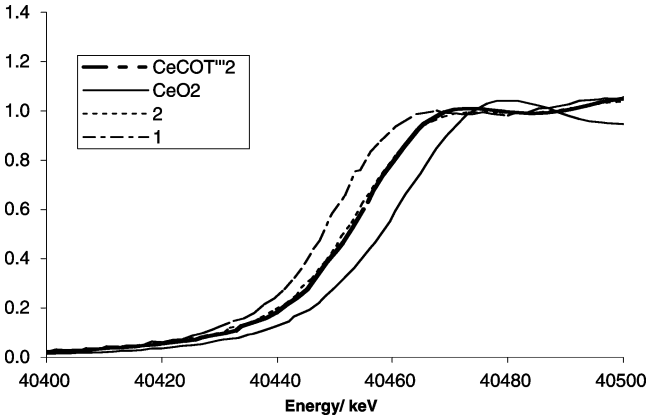

Figure 5. Normalized XANES spectra.

XANES Studies. Figure 5 shows the normalized XANES spectra of the four compounds studied. It is immediately apparent from these data that the absorption edge of CeO_2 is shifted to higher energies than any of the organometallic compounds studied. To quantify this edge shift, we report the

(42) Stultz, S. D.; Andersen, R. A.; Zalkin, A. *Organometallics* **1990**, *9*, 115.

(43) Summerscales, O. T.; Cloke, F. G. N. *Coord. Chem. Rev.* **2006**, *250*, 1122.

Table 3. Summary of XANES Data

compound	edge position/ eV	shift from CeB_6/eV
$Ce(COT'''')_2$	40454.73	4.41
2	40450.49	1.91
1	40450.11	0
CeO_2	40461.41	11.84

Table 4. IE of 2 and Band Assignments

band	assignment	vertical IE	calculated IE
A	$4a_2$	6.32	6.70
B	$4b_1$	6.72	7.14
C	$8b_2$	7.19	7.61
D	$8a_1$	7.53	7.91
E	Si−C	9.1	

Table 5. Relative Energies[a] of $[Ce(C_8H_6)_2]$ Optimized with Different Symmetries[b]

	Δ kJ/mol (B3LYP)	Δ kJ/mol (BP86)
D_2	0.000	0.000
D_{2d}	0.075	1.981
D_{2h}	4.928	15.114

[a] B3LYP with Gaussian and BP86 with ADF. [b] The optimized structure of $[Ce(C_8H_6)_2]$ with the restraints of the D_2 point group has effective D_{2d} symmetry.

edge position in terms of a shift from the edge position of the CeB_6 standard, following the method of Edelstein et al.[10]

These values are reported in Table 3. The shifts from CeB_6 for CeO_2 and $Ce(COT'''')_2$ agree very well with those previously reported,[10] and the values for both **1** and **2** are within the range expected for Ce(III) compounds.

Photoelectron Spectroscopy. He I and He II photoelectron (PE) spectra of **2** are shown in Figure 6, and ionizations energies (IE) of key features are given in Table 4. They resemble closely the PE spectra of the analogous thorium compound reported previously and may be assigned in a similar manner.[44]

The low-energy bands A−D are ill-defined. The presence of two isomers in the gas phase may well be responsible for the broadness of the features. They show an intensity increase relative to band E in the He II spectrum consistent with their assignment to metal ligand bonding orbitals and band E to Si−C ionizations. With respect to each other there is no marked differential intensity change. In general the bands are at lower IE than the corresponding bands in the Th and U analogues, suggesting a weaker interaction of the pentalene ligands with the metal in the Ce compound.[44]

Computational Studies. Density functional theory (DFT) calculations were performed on the model compounds $[Ce(C_8H_6)_2]^x$, where $x = -1$, 0, and $+1$, with the structure constrained to D_{2d} symmetry. The geometry of $[Ce(C_8H_6)_2]$ was also optimized in the D_2, D_{2d} and D_{2h} point groups. The optimized geometry within the restraints of the D_2 point group has effective D_{2d} symmetry; thus the energies of the D_2 and D_{2d} geometries are very close. That of the D_{2h} structure is somewhat higher (Table 5). Thus we may conclude that in the absence of substituents the barrier to relative rotation of the rings is very low and that the preferred geometries are controlled by substituent effects. The calculated geometrical parameters are given in Table 6.

Given the absence of Si^iPr_3 groups on the rings of the model compounds, the agreement between the calculated and experimental structures is excellent. The calculated structural metrics vary little between the neutral molecule and the anion, as is found experimentally. The Ce−C distances increase slightly in the anion. The twist angle is primarily influenced by the substituents, which are neglected in the calculations.

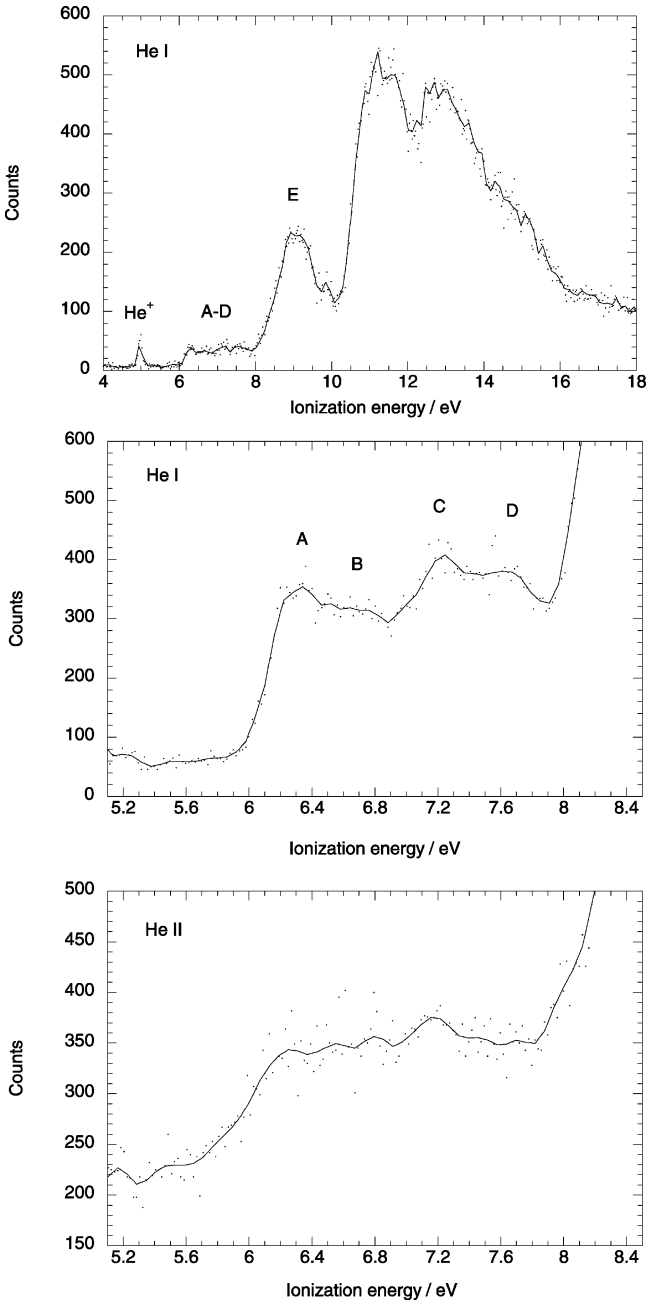

Figure 6. He I and He II PE spectra of $[Ce(C_8H_6)_2]$.

The electronic structure of $[Ce(C_8H_6)_2]$ is similar to that of the Th analogue. Of the eight π orbitals of the pentalene dianion, it is the top two occupied ones, π_4 and π_5, that interact with the metal orbitals, forming bonds of δ symmetry. For a molecular symmetry of D_{2d} they give rise to MOs of symmetry a_2, b_1, b_2, and a_1. The orbital energies and principal AO components of these key orbitals are given in Table 7 for $[Ce(C_8H_6)]_2$. Isosurfaces for LUMO of $[Ce(C_8H_6)]_2$ and the four highest occupied orbitals are given in Figure 7.

The largest single metal contribution is from the Ce 4f:$z(x^2-y^2)$ orbital to the $4a_2$ HOMO, though other metal contributions are also significant.

Calculated IEs are given in Table 4 and agree well with the experimental data given the absence of the Si^iPr_3 substituents in the model. The spacing of the predicted bands corresponds

(44) Cloke, F. G. N.; Green, J. C.; Jardine, C. N.; Kuchta, M. C. *Organometallics* **1999**, *18* (6), 1087.

Table 6. Experimental and Calculated Distances (Å) and Angles (deg) for $[Ce(C_8H_6)_2]$ and $[Ce(C_8H_6)_2]^{-}$[a]

	experimental		calculated	
parameter	$[Ce(C_8H_6)_2]$	$[Ce(C_8H_6)_2]^-$	$[Ce(C_8H_6)_2]$	$[Ce(C_8H_6)_2]^-$
Ce−C(br)	2.495(4)−2.518(13)	2.47(2)−2.592(11)	2.51	2.59
Ce−C(α)	2.730(4)−2.760(11)	2.70(3)−2.88(3)	2.74	2.85
Ce−C(*β*)	2.886(5)−2.925(8)	2.921(11)−2.991(11)	2.88	2.99
C(br)−C(br)	1.3969(9) − 1.46(2)	1.429(10)−1.435(14)	1.46	1.46
C(br)−C(α)	1.425(8)−1.473(7)	1.41(2)−1.46(2)	1.44	1.44
C(α)−C(*β*)	1.366(7)−1.433(17)	1.410(11)−1.439(15)	1.42	1.42
ligand fold	157	158, 159	155.6	159.4
twist angle	85, 33	44, 10	92.28	91.95

[a] The geometric data are from Gaussian (B3LYP) calculations.

Table 7. Fragment Orbital Contributions to Selected MOs of $[Ce(C_8H_6)_2]$[a]

MO	*E* (eV)	% $(Pn)_2$	% Ce	AO-Ce	FO-2×Pn
$10e_1$ (LUMO)	−3.68	0	97	f:*x*	
$4a_2$ (HOMO)	−4.64	66	32	f:$z(x^2-y^2)$	π_5
$4b_1$	−5.15	78	21	d:(x^2-y^2)	π_5
$7b_2$	−5.67	81	18	f:z^3 + d:*xy*	π_4
$7a_1$	−5.96	79	11	d:z^2	π_4

[a] The MOs are labeled according to the symmetry labeling of the D_{2d} point group. Only contributions higher than 5% were considered. The orbital contributions are taken from a fragment calculation in which the molecule was broken in two fragments: a Ce and two pentalenes respectively.

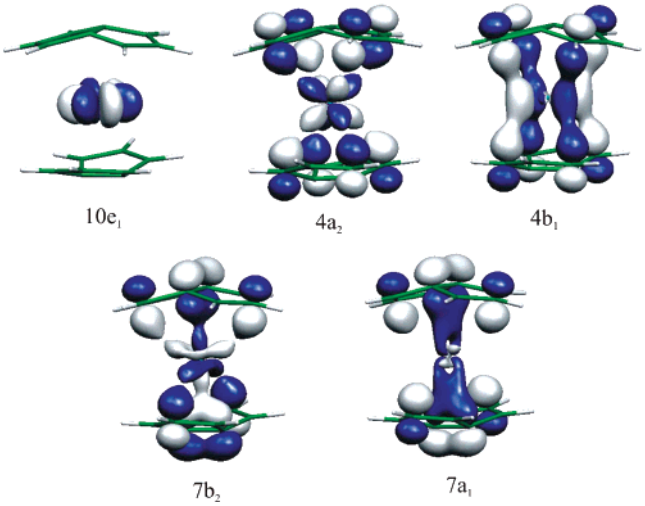

Figure 7. Frontier MOs of $[Ce(C_8H_6)_2]$. The *δ* character of the ligand *π* frontier orbitals, with respect to the metal−ligand axis, closely resembles the e_2 orbitals of $(C_8H_8)^{2-}$.[45]

very well with the experimental spectra. Both Ce 5d and 4f orbitals are expected to show increases in their ionization cross sections with photon energy. The absence of strongly differentiated intensity variations in the PE bands A−D is consistent with the presence of f or d contributions in all four orbitals.

The small HOMO−LUMO gap of $[Ce(C_8H_6)_2]$ (∼1 eV) suggests that the charge-transfer band of **2** at 590 nm may be attributed to excitation from the a_2 HOMO into the f manifold.

It is noteworthy that the 1 and 3 positions that undergo the anomalous chemical shifts are the ones that have significant contributions to the $4a_2$ HOMO and $4b_1$ HOMO−1. It is these orbitals that are most likely to contribute in second-order perturbation theory to the paramagnetic shielding.

Geometry optimization of the anion with the BP86 functional (ADF) leads to a non-aufbau model, as the extra electron is placed in one of the close lying sets of f orbitals. The fragment orbital contributions to the MOs are given in Table 8.

In this unrestricted calculation the corresponding α and *β* spin orbitals have very similar compositions. On reduction, the f orbital contribution to the $4a_2$ and $7b_2$ orbitals decreases significantly, whereas the d contribution to the $4b_1$, $7b_2$, and $7a_1$ orbitals varies little. Overall the metal ligand interaction becomes more ionic. The addition of an f electron to the Ce reduces the polarization of the ligand orbitals and their mixing with metal orbitals.

The consequent charge distribution in the two species may be estimated in a variety of ways. In Table 9 we give results from Mulliken partioning,[46−49] the conventional orbital-based method, and two methods (Hirshfeld[50] and Voronoi[51]) based on density partitioning.

Mulliken population analysis gives a constant charge of +1 for the Ce(III) and Ce(IV) species. The other two methods show a lower overall positive charge on Ce and a slight reduction on addition of the extra electron. The spin density is securely assigned to the Ce in $[Ce(C_8H_6)_2]^-$. The minor calculated charge variation between the neutral molecule and the anion is consistent with the very small shift for the XANES edge between **1** and **2**.

In summary the density functional calculations give a description of the electronic structure of $[Ce(C_8H_6)_2]$ and its anion that agrees very well with experimental probes. The partial covalent character of the four highest occupied MO results in reduction of the charge on Ce below +4 and below that which might reasonably be anticipated for more ionic interactions such as that found in CeO_2. The resultant picture is fully consistent with an oxidation state of IV, which is that arrived at by removal of the ligands with a full shell, in the same way that the oxidation state of Mn in the permanganate ion is VII, although the charge on Mn in no way approaches Mn +7.

Table 8. Fragment Orbital Contributions to Selected MOs of the Anion $[Ce(C_8H_6)_2]^{-}$[a]

	α			*β*			
Irep[b]	*E* (eV)	%Ce	%Pn	Irep[b]	*E* (eV)	%Ce	%Pn
$8b_2$ (α HOMO)	1.798	84.8	9.9				
$8a_1$	1.547	unoc					
$10e_1$	1.134	unoc		$10e_1$ (*β* LUMO)	1.457	unoc	
$4a_2$	−0.349	10.7	80.6	$4a_2$ (*β* HOMO)	−0.306	8.8	82.3
$4b_1$	−0.947	20	72.2	$4b_1$	−0.907	18.3	72.9
$7b_2$	−1.485	11.5	77.0	$7b_2$	−1.445	10.2	78.0
$7a_1$	−1.768	10.7	74.2	$7a_1$	−1.720	10.3	68.5

[a] The contributions are taken from a ADF calculation. The electronic structure is non-aufbau! Unpaired electron of α spin in orbital $8b_2$. [b] Irreducible representation.

Table 9. Charges and Spin Densities (ADF; BP86)

	$[Ce(C_8H_6)_2]$			$[Ce(C_8H_6)_2]^-$			
	Mulliken	Hirshfeld	Voronoi	Mulliken	Hirshfeld	Voronoi	spin dens
Ce	0.98	0.53	0.23	1.00	0.43	0.17	0.97
C (br)	0.08	−0.09	−0.10	0.04	−0.13	-0.13	0.00
C (α)	0.10	−0.07	−0.06	0.07	−0.10	−0.08	0.00
C (*β*)	0.00	−0.06	−0.07	−0.02	−0.08	−0.08	0.00
H (α)	−0.17	0.06	0.09	−0.21	0.03	0.05	0.00
H (*β*)	−0.17	0.06	0.08	−0.22	0.03	0.04	0.00

However, there is clearly more than one possible computational approach. DFT is computationally cheap and has proven to be successful in predicting structure, interpreting electronic and PE spectra, and modeling reactivity in relatively large molecules.[52] However it is restricted to systems that can be described by a single configuration.[53] Such single configuration MO based computational methods are poor at describing relatively weak interactions, the classic example being two H atoms at a long distance where they give equal weight to ionic and neutral forms.[54] Valence bond theory is superior in this respect, as it gives a consistent description of the wave function as distance is varied.[54] The core-like nature of the radial distribution function for 4f electrons, and the presence of a centrifugal barrier that confines them within the core,[55] leads to poor overlap with ligand orbitals. This is accentuated in molecules of high symmetry where hybridization with other metal orbitals is symmetry restricted. The $4a_2$ interaction described above by DFT represents such a case. The alternative way to represent the electronic structure within an MO context is to describe the ground state in terms of configuration interaction between pure ionic configurations, for example, Lf^0d^0, $L^{-1}f^1d^0$, and $L^{-1}f^0d^1$ where L represents the ligand shell and L^{-1} a hole in that shell. The configurations must be of the same symmetry, $^1A_1$, and this requires that the hole in the ligand set of orbitals is of the same symmetry as the Ce localized electron. This is often described as the metal electron being antiferromagnetically coupled to the hole in the ligand shell.[7,8,56] In the case of $[Ce(C_8H_6)_2]$ the DFT description indicates that two configurations would be insufficient, as partial occupation of both f and d orbitals of a_2, b_1, b_2, and a_1 symmetry is required. However the $4a_2$ interaction is unique in that it represents one where symmetry restricts it to an f electron and a ligand set. The dividing line between description of two electrons being antiferromagnetically coupled and forming a covalent bond is difficult to locate; as indicated above, the valence bond description of a chemical bond moves seamlessly between the two. It is a matter of degree. A weaker antiferromagnetic description suggests that a paramagnetic state is likely to be thermally accessible. Covalent bond formation is accompanied by a significant HOMO−LUMO gap. The language used is to a certain extent a matter of training and preference but not a matter for dispute.

However, in a traditional Ce(III) compound with a localized f electron, the characteristics of the f^1 configuration lead to paramagnetism with a moment close to that expected for a free ion in a $^2F_{5/2}$ state.[57] In the case of these formally Ce(IV) compounds such as $CeCOT_2$ and **2**, the ionic configuration endowing Ce^{3+} character to the wave function has the f or d electron spin paired and confined to an orbital of appropriate symmetry. Thus there exists a real distinction between Ce(III) and Ce(IV) compounds whatever the real charge on the metal or the most accurate method of describing the electron distribution. The primary use of an oxidation state classification is to inform as to the potential redox and spectroscopic properties of a metal center. It thus seems appropriate to retain the formal description of these multiconfigurational ground-state species as Ce(IV).

Conclusions

The Ce(III) anionic bis(pentalene) sandwich complex $K[Ce\{C_8H_4(Si^iPr_3\text{-}1,4)_2\}_2]$ (**1**) has been prepared by treatment of $CeCl_3$ with $K_2[C_8H_4(Si^iPr_3\text{-}1,4)_2]$ and crystallographically characterized as its 18-crown-6 complex. Oxidation of **1** with $Ag[BPh_4]$ affords the neutral, formally Ce(IV) sandwich complex $[Ce\{C_8H_4(Si^iPr_3\text{-}1,4)_2\}_2]$ (**2**), whose molecular structure has also been determined. NMR and magnetic studies indicate paramagnetism associated with the Ce. XANES measurements of the K-edge indicate a charge on Ce close to characteristic values for Ce(III) compounds, the excitation energy for **1** being only slightly lower in energy than that found for **2**. PE spectra have been measured and assigned. Density functional calculations give a good account of both the structures and the apparent charge on Ce in **1** and **2** and the photoelectron spectrum of **2**. They also indicate that in a multiconfiguration treatment of the ground state of **2** there is likely to be a contribution from a configuration in which a hole in the ligand shell is strongly antiferromagnetically coupled to an f electron, both the hole and the electron having a_2 symmetry. A classification of a formal oxidation state of IV is recommended for **2**.

Acknowledgment. We gratefully acknowledge EPSRC for partial financial support of this project. We thank the Humboldt Foundation for a Fellowship (G.B.) and the Oxford Supercomputing Centre for provision of computing time.

Note Added in Proof. The permethylated pentalene analog of **2** has recently been reported: Ashley, A.; Balazs, G.; Cowley, A.; Green, J. C.; Booth, C. H.; O'Hare, D. *Chem. Commun.* **2007**, 1515.

Supporting Information Available: Complete crystallographic details of the X-ray structures of **1** and **2**. This material is available free of charge via the Internet at http://pubs.acs.org.

OM7002738

(45) Cloke, F. G. N.; Green, J. C.; Jardine, C. N. *Organometallics* **1999**, *18*, 1087.
(46) Mulliken, R. S. *J. Chem. Phys.* **1955**, *23*, 1833.
(47) Mulliken, R. S. *J. Chem. Phys.* **1955**, *23*, 1841.
(48) Mulliken, R. S. *J. Chem. Phys.* **1955**, *23*, 2338.
(49) Mulliken, R. S. *J. Chem. Phys.* **1955**, *23*, 2343.
(50) Hirshfeld, F. L. *Theor. Chim. Acta* **1977**, *44* (2), 129.
(51) Fonseca Guerra, C.; Handgraaf, J.-W.; Baerends, E. J.; Bickelhaupt, F. M. *J. Comput. Chem.* **2004**, *25*, 189.
(52) Ziegler, T. *Chem. Rev.* **1991**, *91*, 7401.
(53) Kohn, W.; Sham, L. J. *Phys. Rev. A* **1965**, *140*, 1133.
(54) Coulson, C. A. *Valence*, 2nd ed.; OUP: Oxford, 1961.
(55) Cowan, R. D. *The Theory of Atomic Structure and Spectra*; University of California Press: Berkeley, 1981.
(56) Dolg, M.; Wedig, U.; Stoll, H.; Preuss, H. *J. Chem. Phys.* **1987**, *86*, 866.
(57) Figgis, B. N. *Introduction to Ligand Fields*; Wiley: New York, 1966.